CRYSTAL GROWTH & DESIGN

Communication

pubs.acs.org/crystal

# $Ni(NO_3)_2$-Assisted Catalytic Synthesis and Photoluminescence Property of Ultralong Single Crystal Sialon Nanobelts

Juntong Huang,[†,‡] Yan'gai Liu,[†] Zhaohui Huang,*[,†] Minghao Fang,[†] Shaowei Zhang,*[,‡,§] Wei Xie,[‡] Jingzhou Yang,[†] Saifang Huang,[†] and Youguo Xu[†]

[†]School of Materials Science and Technology, China University of Geosciences (Beijing), Beijing 100083, P. R. China

[‡]Department of Materials Science and Engineering, University of Sheffield, Sheffield S1 3JD, U.K.

[§]College of Engineering, Mathematics and Physical Sciences, University of Exeter, Exeter EX4 4QF, U.K.

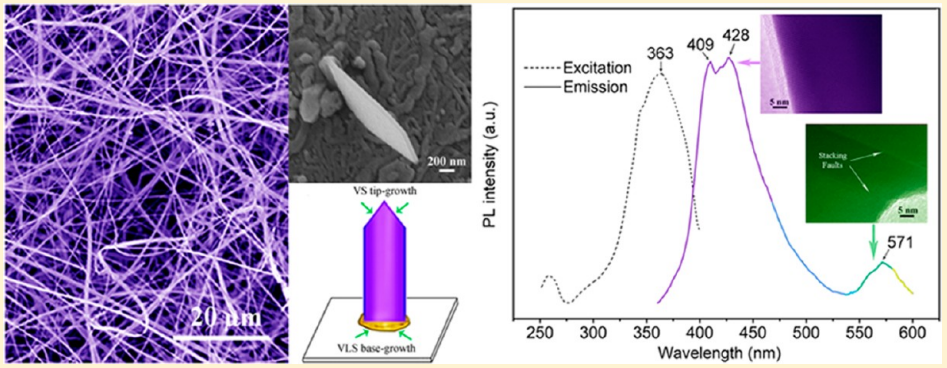


**ABSTRACT:** Ultralong single crystal Sialon nanobelts were prepared on a graphite cover coated with $Ni(NO_3)_2$ by facile thermal chemical vapor deposition reactions of Si, Al, and $Al_2O_3$ with flowing $N_2$ at 1450 °C. The as-synthesized Sialon nanobelts were up to several millimeters long and several hundred nanometers wide, and they had width/thickness ratios of 5−15. Their growth process was codominated by a Ni-catalytic vapor−liquid−solid (VLS) base-growth mechanism and a vapor−solid (VS) tip-growth mechanism. The former was responsible for the initial nucleation and proto-nanobelt formation of Sialon and the subsequent growth along the [100] direction, and the latter additionally contributed the growth at tips. The room-temperature photoluminescence (PL) spectrum showed that the as-synthesized Sialon nanobelts had a special emission with two maximum peaks at 409 nm (3.03 eV) and 428 nm (2.90 eV) located in the violet-blue spectral range, making possible potential applications in LED and optoelectronic nanodevices.

Belt-like nanostructured materials have attracted considerable attention because of their novel morphologies, excellent physical properties, and great potential for wide applications.[1,2] Compared to a cylindrical nanomaterial (e.g., nanowire, nanorod, and nanotube), a nanobelt possesses a rectangle-like cross section with additional large width-to-thickness ratio. Since semiconducting oxide nanobelts were first discovered by Wang et al. in 2001,[1] various material types of nanobelts have been successfully synthesized, including metals (Au, Ni, Ag),[3] oxides ($Co_3O_4$, $V_2O_5$, $Bi_2O_3$),[4] sulfides (ZnS, CdS),[5] carbides (SiC, $Al_4C_3$),[6] nitrides (GaN, InN, $Si_3N_4$),[7] and other multicomponents.[8]

Sialon represents a group of materials with both excellent properties and unique structural features, based on the $Si_3N_4$ structure, where Si−N bonds are partially replaced by Al−O bonds, respectively.[9] Such replacements only increase the crystal unit sizes without changing the whole crystal structure. In some cases, charge balance is achieved by interstitial solution of rare earth (RE) ions ($Eu^{2+}$, $Nd^{3+}$, $Ce^{3+}$, $Dy^{3+}$, $Pr^{3+}$, *etc.*).[10] Such RE-doped Sialon possesses tailored optical-electrical properties, thus having a potential application in functional devices, such as white light LEDs and solid-state lasers.[10] Similar to the III−N compounds, Sialon could be used as an excellent host material in terms of high dopant concentration, good mechanical/thermal properties, and chemical stability. In recent years, great progress has been made in producing bulk materials of Sialon as well as their whiskers/fibers/tubes.[11] Nevertheless, studies on the synthesis of Sialon nanobelts are still lacking. So far, only one relevant technique based on the pyrolysis and nitridation of expensive SiONCH−Al polymeric precursors has been attempted.[12] With this technique, high-yield Sialon nanobelts could be produced. However, this technique suffered from several disadvantages, including the high cost of raw materials, a long and complex process, as well as disadvantages affecting the quality of the resultant nanobelts. For example, significant amorphous carbon from the pyrolysis process of polymeric precursors remained in the final product. Some nanobelts were deeply rooted or embedded in the

**Received:** September 25, 2012
**Revised:** November 22, 2012
**Published:** December 7, 2012

remaining powder mixtures after synthesis, leading to additional difficulties in separation/purification for future applications.

In this communication, we report a facile approach via thermal chemical vapor deposition (CVD) reactions of Si, Al, and $Al_2O_3$ powders to synthesize high-yield Sialon nanobelts on a graphite felt precoated with a nickel nitrate catalyst. The as-synthesized nanobelts were fully characterized and their photoluminescence properties examined. It is worth mentioning that our method is relatively low cost and green because of using relatively inexpensive and environmentally friendly inorganic material precursors. The nanobelt products are formed on the carbon felt substrate separated away from the starting raw materials, avoiding difficulties in separation/purification.

In a typical preparation procedure (the experimental setup shown in Scheme 1), Si, Al, and $Al_2O_3$ raw material powders were weighed based on the composition of $\beta$-Sialon ($Si_{6-z}Al_zO_zN_{8-z}$) with $z$ = 2, followed by 1 h of mixing and milling in a ball mill. About 2 g of the mixed batch was loaded in a corundum boat placed in the center of a long corundum tube inserted in an electric furnace. A graphite felt was coated with a 0.1 g·$L^{-1}$ nickel nitrate solution, dried in oven at 100 °C, and then used to cover the corundum boat, about 1 cm away from the raw materials. The tube was purged 5 times with $N_2$ to remove the air, and then it was heated from room temperature to 1450 °C at 2 °C·$min^{-1}$ and held for 3 h in flowing $N_2$ (purity 99.999%). The fired samples were allowed to furnace-cool to room temperature at 3 °C·$min^{-1}$. A white layer of product was visually seen on the underside of the graphite cover. It was characterized with an X-ray diffractometer (XRD, D8 Advance, Germany), a scanning electron microscope (SEM, JEOL JSM-7001F, Japan) equipped with an energy dispersive spectroscope (EDS, INCA), and a high-resolution transmission electron microscope (HRTEM) (JEOL JEM-2100, Japan). The room-temperature photoluminescence (PL) spectra of the products were recorded with a fluorescence spectrophotometer (Edinburgh, FLSP-920, U.K.) equipped with a 450 W xenon discharge lamp as the excitation source.

XRD (Figure 1a) identifies that the products grown on the graphite cover are hexagonal $Si_4Al_2O_2N_6$ with lattice constants of $a$ = 7.643 Å and $c$ = 2.945 Å [JCPDS card No. 76-599, space group, $P6_3/m$ (No. 176)]. Low-magnification SEM images (Figure 1b and c) reveal that they exhibit one-dimension structures, typically several hundred micrometers to several millimeters in length. A high-magnification SEM image (Figure 1d–f) further reveals that they actually are nanobelts with widths of 300–1000 nm, and width to thickness ratios of 5–15. Many of the nanobelts are highly curved, indicating good flexibility. The composition of the nanobelts in terms of EDS is 30.2% Si, 15.6% Al, 15.9% O, and 38.3% N (atomic ratio) (Figure 1g), close to the stoichiometric composition of $Si_4Al_2O_2N_6$.

**Scheme 1. Schematic Experimental Setup for Sialon Nanobelts Synthesis**

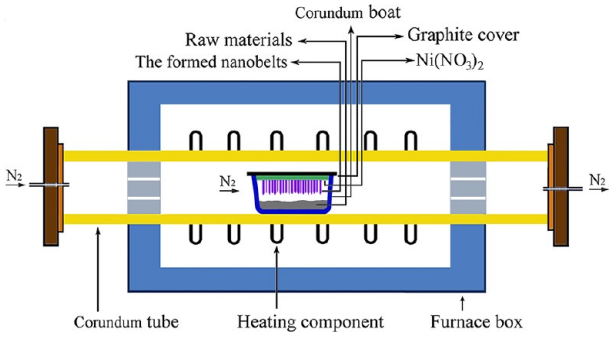


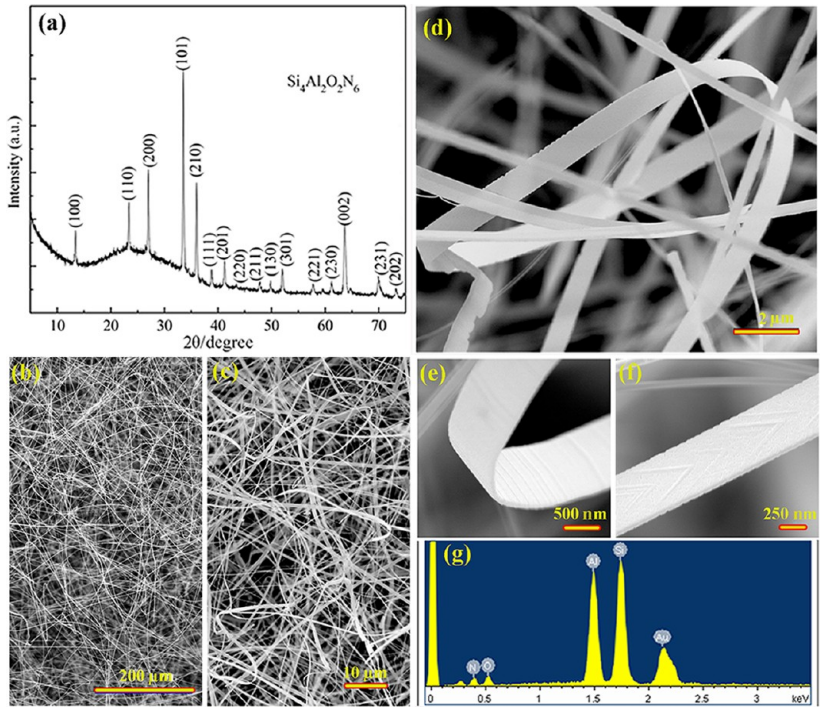


**Figure 1.** (a) XRD pattern. (b, c) Low-magnification SEM images of the as-synthesized products. (d) High-magnification SEM image of the as-synthesized products. (e) Curved and (f) straight nanobelt. (g) EDS pattern of the nanobelt.


dx.doi.org/10.1021/cg301399a | *Cryst. Growth Des.* 2013, 13, 10–14

The detailed morphology and crystalline structure of the Sialon nanobelts were further characterized by TEM and HRTEM. Figure 2a and b shows the typical belt-like geometry

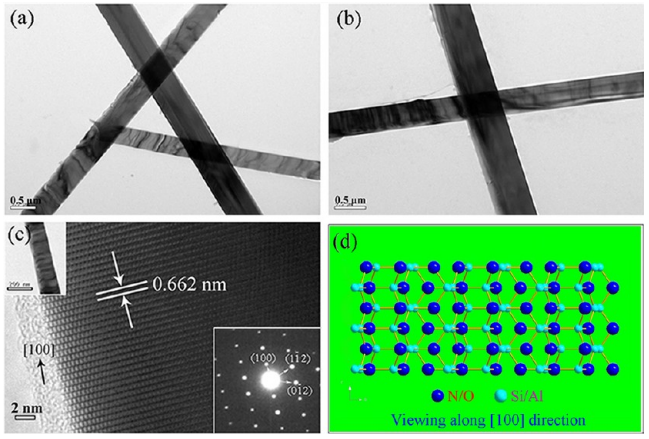


**Figure 2.** (a, b) TEM images and (c) HRTEM images of the as-synthesized products. The inset in the lower right side of (c) shows the corresponding SAED pattern. (d) Atomic model of hexagonal structures of Sialon nanobelts viewed along the [100] direction.

of the products, and each nanobelt has a uniform width along its length. The HRTEM lattice images (Figure 2c) reveal that the nanobelts possess a perfect crystal structure, and the corresponding selected area electron diffraction (SAED) patterns (the insets in Figure 2c) further verify their hexagonal single crystal structure. The marked interplanar *d*-spacing in Figure 2c, *ca.* 0.662 nm, matches well with the (100) lattice plane of Sialon. These lattice fringes, along with the SAED patterns, suggest that [100] is the growth direction of the Sialon nanobelts. The atomic model of Sialon nanobelts along the [100] is illustrated in Figure 2d, revealing that the side surfaces are polar and are terminated with either Si/Al or O/N. In addition, a few Sialon nanobelts exhibit distinctive defect morphologies, containing numerous stacking faults with the width of ~18 nm (Figure 3).

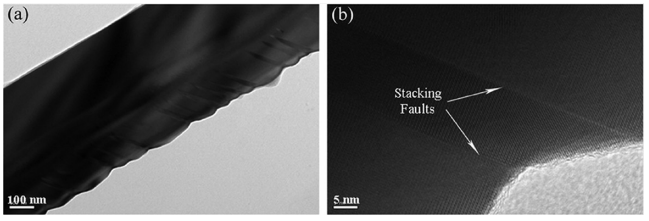


**Figure 3.** (a) TEM and (b) HRTEM of a nanobelt with many stacking faults.

For comparison and identification of the catalytic effect of nickel nitrate, a graphite felt without catalyst deposition was also tested under the identical conditions. In this case, instead of nanobelts, only Sialon nanowires were generated (Figure 4). This indicates that the catalyst plays a key role in the growth process of Sialon nanobelts. To further clarify the role, some short Sialon nanobelts having just started to grow from the underside of the graphite cover were characterized (Figure 5), which could give some useful clues about the initial growth process on the graphite cover. Their main bodies and tips contained only Si, Al, O, and N but did not contain any Ni, as

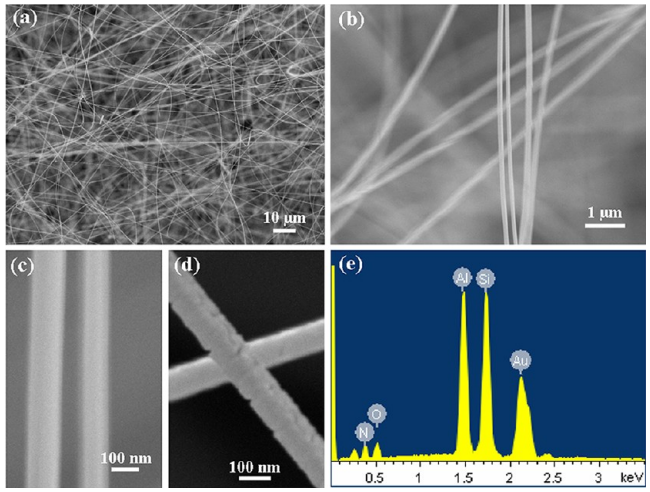


**Figure 4.** SEM images (a–d) and EDS pattern (e) of the products on the underside of the graphite cover without catalyst deposition, revealing they are Sialon nanowires rather than Sialon nanobelts formed with $Ni(NO_3)_2$.

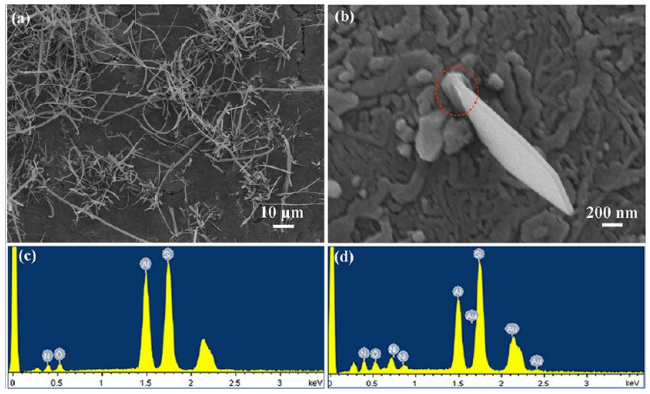


**Figure 5.** (a and b) SEM images of Sialon nanobelts grown from the $Ni(NO_3)_2$-coated graphite cover in the initial stage. (c and d) EDS patterns of the tip and root of the Sialon nanobelt in part b, respectively.

revealed by EDS (Figure 5c), implying that the overall growth process might not have been dominated by the well documented vapor–liquid–solid (VLS) tip-growth mechanism. Interestingly, at the roots of the short nanobelts (marked by the dotted rings in Figure 5b), Ni was detected (Figure 5d), suggesting that new mechanisms could have been involved, which can be schematically illustrated in Scheme 2 and discussed as follows.

According to thermodynamic calculations, $Ni(NO_3)_2$ remaining on the graphite cover would start to decompose and form NiO particles at 260 °C (eq 1).[13] Subsequently, the formed NiO particles would be reduced to Ni particles by carbon from the graphite cover surface (eq 2, Scheme 2a), which offered catalytically active sites for the nucleation and growth of the nanobelts.

$$2Ni(NO_3)_2 \rightarrow 2NiO + 4NO_2 + O_2 \quad (1)$$

$$2NiO + C \rightarrow 2Ni + CO_2 \quad (2)$$

At the test temperature (1450 °C), vapor phases would be generated from the raw materials via the following:[14]

**Scheme 2. Newly Proposed Mechanism for the Growth of Sialon Nanobelts**

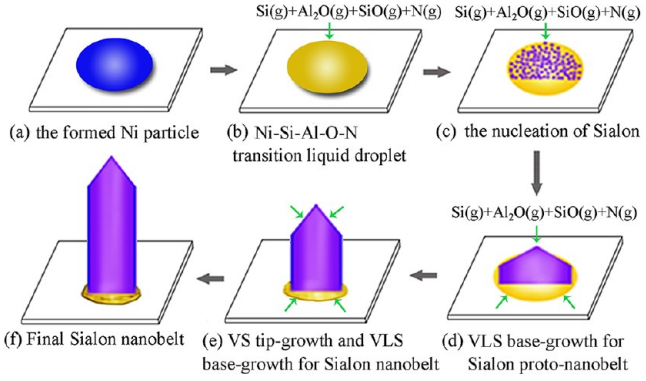


$$2Si_{(s)} + Al_2O_{3(s)} \rightarrow 2SiO_{(g)} + Al_2O_{(g)} \quad (3)$$

$$4Al_{(l)} + Al_2O_{3(g)} \rightarrow 3Al_2O_{(g)} \quad (4)$$

$$Si_{(s)} \rightarrow Si_{(g)} \quad (5)$$

these vapor phases could diffuse to the Ni particles formed earlier on the graphite cover, forming eutectic Ni−Si−Al−O−N liquid droplets (Scheme 2b). Upon saturation with the composition of Si−Al−O−N, the nucleation would start in those liquid droplets, then followed by the formation of the proto-nanobelts (small nanobelts "template") of Sialon (eq 6, Scheme 2c). Considering that nickel was only detected in the roots of the nanobelts rather than in their tips, the VLS base-growth mechanism instead of the VLS tip-growth mechanism should have dominated the nanobelt growth process (Scheme 2d). For the VLS base-growth mechanism to function, the bonding between the catalyst and the substrate needs to be strong.[15] Although the interaction between the two in the present case was not fully understood, the bonding between them is believed to be strong, considering the good wettability of liquid Ni on graphite (with a contact angle of 45°)[16] and the good connection between the nanobelt root and the substrate (Figure 5b). After initial proto-nanobelt formation, gaseous SiO, $Al_2O$, Si, and N would continue to come to the catalyst droplets, sustaining the growth of Sialon. Moreover, considering the triangular tips of the nanobelts (Figure 5b), the VS mechanism also could have contributed to the tip-growth of the Sialon nanobelts, after they had grown out from the droplets (Scheme 2e). In this case, those gaseous phases continued to diffuse to the tips and react to deposit Sialon there (eq 7), additionally accelerating the growth along the length direction. The formation of nanobelts instead of nanowires is attributed to the nonuniformity of radial growth as well as the much faster axial growth than radial growth, as suggested by many other researchers.[17] The combination of the two mechanisms explained the formation of the long single crystal Sialon nanobelts with the present work (Scheme 2f).

$$[SiO]_{(l)} + [Al_2O]_{(l)} + 3[Si]_{(l)} + 6[N]_{(l)} \rightarrow Si_4Al_2O_2N_{6(s)} \quad \text{(base-growth)} \quad (6)$$

$$SiO_{(g)} + Al_2O_{(g)} + 3Si_{(g)} + 3N_{2(g)} \rightarrow Si_4Al_2O_2N_{6(s)} \quad \text{(tip-growth)} \quad (7)$$

The room-temperature PL spectra of the Sialon nanobelts are shown in Figure 6. There is a special emission ranging from

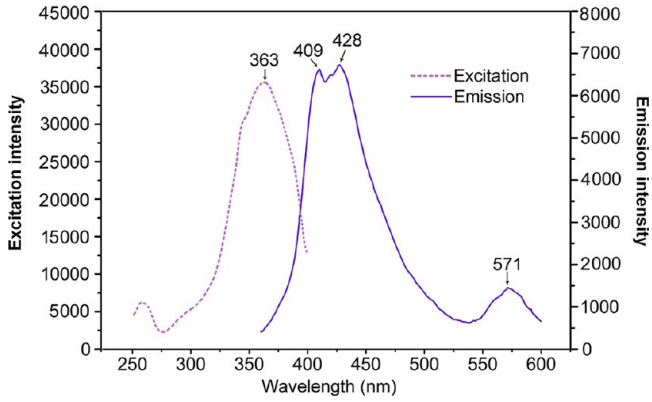


**Figure 6.** Excitation and emission spectra of Sialon nanobelts. The emission spectrum was measured with excitation at 310 nm, and the excitation spectrum was monitored at 428 nm.

around 380 to 500 nm with two maximun peaks at 409 nm (3.03 eV) and 428 nm (2.90 eV) located in the violet/blue spectral range, which can be reasonably attributed to the cation cavity and sublattices migration resultant from the replacement of the Si−N bond by the Al−O bond.[12] However, the emission range of Sialon nanobelts with $z = 2$ in this work is strikingly different from that of the nanobelts with $z = 1$ (an orange/red emission range (600−700 nm) centered at 652 nm) reported by Qin et al.[12] This difference is related to the O/N ratio of the as-synthesized Sialon. The O/N ratio increases when the $z$ value increases, leading to reduction of the covalence of Sialon. The reduction in the covalent bonding would cause a blue-shift of the emission band.[18] Moreover, a small peak centered at 571 nm also appears, which can be ascribed to the emission of crystal stacking faults.[19] Since those stacking faults would introduce electronic energy levels, they may participate in optical transitions and, consequently, resulted in the photoluminescence.[20] Nevertheless, the exact luminescence mechanism of Sialon nanobelts still needs to be further investigated.

In summary, ultralong single crystal Sialon nanobelts have been successfully synthesized via a thermal catalytic chemical vapor deposition route using Si, Al, and $Al_2O_3$ as raw materials. The as-synthesized nanobelts were up to several millimeters long and several hundred nanometers wide, and they had width/thickness ratios of 5−15. Their growth direction was along [100]. Most of them were fault-free, exhibiting regular stacking sequences, but some contained numerous stacking faults. The growth process was codominated by VLS base-growth and VS tip-growth mechanisms. The as-synthesized Sialon nanobelts generated a special violet/blue emission, making possible potential applications in optoelectronic nanodevices and LED materials.

## AUTHOR INFORMATION


### Corresponding Author

*Z.H.: Tel, +8610 8232 2186; e-mail, huang118@cugb.edu.cn; web, http://www.cugb.edu.cn/profHomepage.action? zgh=2004011828. S.Z.: Tel, +44 13 9272 5276; e-mail, s.zhang@sheffield.ac.uk; web, http://emps.exeter.ac.uk/engineering/staff/sz268.


### Notes

The authors declare no competing financial interest.

## ■ ACKNOWLEDGMENTS

This work was financially supported by the National Natural Science Foundation of China (Grant Nos. 51032007 and 50972134) and the New Star Technology Plan of Beijing (Grant No. 2007A080). J.H. would like to thank the China Scholarship Council, and Z.H. would like to acknowledge support by a Gledden Visiting Senior Fellowship from the University of Western Australia in 2010.

## ■ REFERENCES

(1) Pan, Z. W.; Wang, Z. L. *Science* **2001**, *291* (5510), 1947−1949.
(2) (a) Du, W.; Zhu, J.; Li, S.; Qian, X. *Cryst. Growth Des.* **2008**, *8* (7), 2130−2136. (b) Jiao, L.; Wang, X.; Diankov, G.; Wang, H.; Dai, H. *Nat. Nanotechnol.* **2010**, *5* (5), 321−325. (c) Qu, Y. Q.; Bai, J.; Liao, L.; Cheng, R.; Lin, Y. C.; Huang, Y.; Guo, T.; Duan, X. *Chem. Commun.* **2011**, *47* (4), 1255−1257. (d) Chen, L.; Hernandez, Y.; Feng, X.; Müllen, K. *Angew. Chem., Int. Ed.* **2012**, *51* (31), 7640−7654.
(3) (a) Chen, Y.; Somsen, C.; Milenkovic, S.; Hassel, A. W. *J. Mater. Chem.* **2008**, *19* (7), 924−927. (b) Liu, Z. P.; Li, S.; Yang, Y.; Peng, S.; Hu, Z.; Qian, Y. T. *Adv. Mater.* **2009**, *311* (8), 2474−2479. (c) Liu, L.; Yoo, S. H.; Lee, S. A.; Park, S. *Cryst. Growth Des.* **2011**, *11* (9), 3731−3734.
(4) (a) Tian, L.; Zou, H.; Fu, J.; Yang, X.; Wang, Y.; Guo, H.; Fu, X.; Liang, C.; Wu, M.; Shen, P. K. *Adv. Funct. Mater.* **2010**, *20* (4), 617−623. (b) Wang, H.-G.; Ma, D.-L.; Huang, Y.; Zhang, X. B. *Chem.—Eur. J.* **2012**, *18* (29), 8987−8993. (c) Zheng, F. L.; Li, G. R.; Ou, Y. N.; Wang, Z. L.; Su, C. Y.; Tong, Y. X. *Chem. Commun.* **2010**, *46* (27), 5021−5023.
(5) (a) Wang, Z.; Daemen, L. L.; Zhao, Y.; Zha, C.; Downs, R. T.; Wang, X.; Wang, Z. L.; Hemley, R. J. *Nat. Mater.* **2005**, *4* (12), 922−927. (b) Fan, X.; Zhang, M. L.; Shafiq, I.; Zhang, W. J.; Lee, C. S.; Lee, S. T. *Cryst. Growth Des.* **2009**, *9* (3), 1375−1377.
(6) (a) Xi, G.; Peng, Y.; Wan, S.; Li, T.; Yu, W.; Qian, Y. *J. Phys. Chem. B* **2004**, *108* (52), 20102−20104. (b) Sun, Y.; Cui, H.; Gong, L.; Chen, J.; Shen, P.; Wang, C. *Nanoscale* **2011**, *3* (7), 2978−2982.
(7) (a) Xue, S.; Zhang, X.; Huang, R.; Tian, D.; Zhuang, H.; Xue, C. *Cryst. Growth Des.* **2008**, *8* (7), 2177−2181. (b) Hu, M. S.; Wang, W. M.; Chen, T. T.; Hong, L. S.; Chen, C. W.; Chen, C. C.; Chen, Y. F.; Chen, K. H.; Chen, L. C. *Adv. Funct. Mater.* **2005**, *16* (4), 537−541. (c) Huang, J. T.; Zhang, S. W.; Huang, Z. H.; Wen, Y.; Fang, M. H.; Liu, Y. G. *CrystEngComm* **2012**, *14* (21), 7301−7305.
(8) (a) Zhang, X.; Xu, Z.; Tang, S.; Deng, Y.; Du, Y. *Cryst. Growth Des.* **2011**, *11* (7), 2852−2857. (b) Sun, X. P.; Hagner, M. *Chem. Mater.* **2008**, *20* (9), 2869−2871. (c) Li, L.; Lee, P. S.; Yan, C.; Zhai, T.; Fang, X.; Liao, M.; Koide, Y.; Bando, Y.; Golberg, D. *Adv. Mater.* **2010**, *22* (45), 5145−5149. (d) Chithaiah, P.; Chandrappa, G.; Livage, J. *Inorg. Chem.* **2012**, *51* (4), 2241−2246. (e) Kiatkittipong, K.; Ye, C.; Scott, J.; Amal, R. *Cryst. Growth Des.* **2010**, *10* (8), 3618−3625.
(9) (a) Hampshire, S.; Park, H.; Thompson, D.; Jack, K. *Nature* **1978**, *274* (5674), 880−882. (b) Zerr, A.; Riedel, R.; Sekine, T.; Lowther, J. E.; Ching, W. Y.; Tanaka. *Adv. Mater.* **2006**, *18* (22), 2933−2948.
(10) (a) Kimoto, K.; Xie, R. J.; Matsui, Y.; Ishizuka, K.; Hirosaki, N. *Appl. Phys. Lett.* **2009**, *94* (4), 041908−3. (b) Huang, S. F.; Huang, Z. H.; Fang, M. H.; Liu, Y. G.; Huang, J. T.; Yang, J. Z. *Cryst. Growth Des.* **2010**, *10* (6), 2439−2442. (c) Huang, J. T.; Zhou, H. P.; Huang, Z. H.; Liu, G. H.; Fang, M. H.; Liu, Y. G. *J. Am. Ceram. Soc.* **2012**, *95* (6), 1871−1877. (d) Liu, T. C.; Cheng, B. M.; Hu, S. F.; Liu, R. S. *Chem. Mater.* **2011**, *23* (16), 3698−3705.
(11) (a) Ng, D. H. L.; Cheung, T. L. Y.; Kwong, F.; Li, Y. F.; Yang, R. *Mater. Lett.* **2008**, *62* (8), 1349−1352. (b) Hou, X. M.; Yu, Z. Y.; Chen, Z. Y.; Zhao, B. J.; Chou, K. C. *Dalton Trans.* **2012**, *41* (23), 7127−7133. (c) Shen, Z. J.; Zhao, Z.; Peng, H.; Nygren, M. *Nature* **2002**, *417* (6886), 266−269. (d) Liu, G. H.; Chen, K. X.; Li, J. T. *CrystEngComm* **2012**, *14* (17), 5585−5588.
(12) Qin, C. L.; Wen, G. W.; Wang, X. Y.; Song, L.; Huang, X. X. *J. Mater. Chem.* **2011**, *21* (16), 5985−5991.
(13) Kim, T. Y.; Lee, S. H.; Mo, Y. H.; Nahm, K. S.; Kim, J. Y.; Sun, E. K.; Kim, M. *Korean J. Chem. Eng.* **2004**, *21* (3), 733−738.
(14) (a) Ksiazek, M.; Sobczak, N.; Mikulowski, B.; Radziwill, W.; Surowiak, I. *Mater. Sci. Eng., A* **2002**, *324* (1), 162−167. (b) Fang, X. S.; Ye, C. H.; Zhang, L. D.; Xie, T. *Adv. Mater.* **2005**, *17* (13), 1661−1665. (c) Dong, P. L.; Wang, X. D.; Zhang, M.; Guo, M.; Seetharaman, S. *J. Nanomater.* **2008**, *2008*, 282187.
(15) Kumar, M.; Ando, Y. *J. Nanosci. Nanotechnol.* **2010**, *10* (6), 3739−3758.
(16) Bozack, M.; Swanson, L.; Bell, A. *J. Mater. Sci.* **1987**, *22* (7), 2421−2430.
(17) (a) Xu, B. S.; Yang, D.; Wang, F.; Liang, J.; Ma, S. F. *Appl. Phys. Lett.* **2006**, *89* (7), 074106−3. (b) Yang, W. Y.; Xie, Z. P.; Miao, H. Z.; Zhang, L. G.; Ji, H.; An, L. N. *J. Am. Ceram. Soc.* **2008**, *88* (2), 466−469.
(18) (a) Ryu, J. H.; Park, Y. G.; Won, H. S.; Kim, S. H.; Suzuki, H.; Yoon, C. *J. Cryst. Growth* **2009**, *311* (3), 878−882. (b) Xie, R. J.; Hirosaki, N. *Sci. Technol. Adv. Mater.* **2007**, *8* (7), 588−600.
(19) (a) Liu, R.; Bell, A.; Ponce, F.; Chen, C.; Yang, J.; Khan, M. A. *Appl. Phys. Lett.* **2005**, *86* (2), 021908−3. (b) Gu, Z. J.; Paranthaman, M. P.; Pan, Z. W. *Cryst. Growth Des.* **2008**, *9* (1), 525−527.
(20) Tham, D.; Nam, C. Y.; Fischer, J. E. *Adv. Funct. Mater.* **2006**, *16* (9), 1197−1202.